Advances in Water Resources 108 (2017) 423–438

Contents lists available at ScienceDirect

Advances in Water Resources

journal homepage: www.elsevier.com/locate/advwatres

Using remote sensing and modeling techniques to investigate the annual parasite incidence of malaria in Loreto, Peru

Aneela Mousam[a,*], Viviana Maggioni[a], Paul L. Delamater[b], Antonio M. Quispe[c]

[a] George Mason University, Department of Civil, Environmental, and Infrastructure Engineering, Fairfax, VA, United States
[b] George Mason University, Department of Geography and GeoInformation Science, Fairfax, VA, United States
[c] Johns Hopkins Bloomberg School of Public Health, Baltimore, MD, United States

ARTICLE INFO

Article history:
Received 10 May 2016
Revised 9 November 2016
Accepted 18 November 2016
Available online 19 November 2016

Keywords:
Malaria
Peru
Climate
Environment
Remote sensing
Modeling

ABSTRACT

Between 2001 and 2010 significant progress was made towards reducing the number of malaria cases in Peru; however, the country saw an increase between 2011 and 2015. This work attempts to uncover the associations among various climatic and environmental variables and the annual malaria parasite incidence in the Peruvian region of Loreto. A Multilevel Mixed-effects Poisson Regression model is employed, focusing on the 2009–2013 period, when trends in malaria incidence shifted from decreasing to increasing. The results indicate that variations in elevation ($\beta = 0.78$; 95% confidence interval (CI), 0.75–0.81), soil moisture ($\beta = 0.0021$; 95% CI, 0.0019–0.0022), rainfall ($\beta = 0.59$; 95% CI, 0.56–0.61), and normalized difference vegetation index ($\beta = 2.13$; 95% CI, 1.83–2.43) is associated with higher annual parasite incidence, whereas an increase in temperature ($\beta = -0.0043$; 95% CI, -0.0044–-0.0041) is associated with a lower annual parasite incidence. The results from this study are particularly useful for healthcare workers in Loreto and have the potential of being integrated within malaria elimination plans.

1. Introduction

Malaria continues to be one of the most severe public health problems worldwide. According to the World Health Organization (WHO, 2015), 1.2 billion people are at a high risk of being infected with malaria and developing the disease and 214 million cases were reported in 2015. The majority of the cases occurred in Africa and South-East Asia, but transmission continues in several parts of South America as well (WHO, 2015). In 2012, approximately 25% of the malaria burden in South America was experienced by 12 municipalities in Peru, Brazil, and Venezuela (Zaitchik et al., 2012).

Peru is making progress towards controlling malaria but has not been able to completely eliminate the disease, thus making it the country with the second highest number of malaria cases in South America (Bautista et al., 2006; WHO, 2015). In 2015, Peru had an estimated population of 30,973,148, of which 12,165,089 had at least some risk of contracting malaria (WHO, 2015). During the 1990s, there was a 7-fold increase in malaria incidence in Peru, rising from 13 per 10,000 inhabitants in 1990 to a peak of 88 per 10,000 in 1996 (Roper et al., 2000). Specifically, over 60% of all malaria cases occurred in the Loreto Department of Peru (Zaitchik et al., 2012). As a result, the Loreto has been the major focus of the malaria control. In 1990, there were only 641 cases in Loreto, but the number rose to 121,268 cases by 1997 (Roper et al., 2000). Peru saw an overall decline in malaria cases from 2001–2010, but the number of cases has increased since then, especially in Loreto. In 2015, there were nearly 3 times as many malaria cases as were reported in 2011.

Peru has implemented a number of initiatives in an effort to control malaria. The Peruvian Malaria Program provides free antimalarial drugs under a Directly Observed Therapy (DOT) protocol (Chuquiyauri et al., 2012). In addition, regional efforts to improve malaria surveillance, early detection, prompt treatment, and vector management have been employed since 2000 (Herrera et al., 2012). From 2006 to 2011, Peru participated in the PAMAFRO project, a malaria control program in which long lasting insecticide-impregnated nets (LLIN) were delivered to remote communities in Loreto. Based on the most recent project report (PAMAFRO, 2010), most of the LLINs were distributed during the first years of the project (prior to 2009). Despite these efforts and increased funding for malaria control in the region, there are still gaps in understanding how different factors impact malaria transmission and elimination (Herrera et al., 2012). This brings into question the role of climate and environmental factors.

In Peru, the two main Anopheles species responsible for malaria transmission are the *An. darlingi* (along the Amazon basin) and *An. pseudopunctipennis* (along the Peruvian north coast)

* Corresponding author.
E-mail address: aneelamousam90@gmail.com (A. Mousam).

https://doi.org/10.1016/j.advwatres.2016.11.009
0309-1708/

(Sinka et al., 2012) The seasonality patterns of the mosquito are closely related to the rainfall cycle, mainly due to rainfall increasing the availability of breeding sites leading to peak abundances of *An. darlingi* reported in the rainy season (Reinbold-Wasson et al., 2012). The larvae also require stable conditions in the breeding sites and prefer large water bodies such as rivers. Additionally, the mosquitoes prefer certain amount of vegetation coverage and temperatures ranging from 20 to 28 °C (Hiwat and Bretas, 2011). The changing temperature trends can impact the time needed for parasite development, mosquito abundance, gonotrophic cycle, and larval development (Patz and Olson, 2006). Past studies clearly indicate that global climate variability already has and will continue to have an impact on malaria transmission. Specifically, climatic variations and extreme weather events have been shown to have a profound impact on infectious agents and their associated vector organisms (Parham and Michael, 2010; Patz et al., 2005). These two studies also showed that vectors such as mosquitoes are devoid of thermostatic mechanisms, so their reproduction and survival rates are strongly impacted by fluctuations in temperature. Parham and Michaels (2010) showed that environmental variables such as temperature, humidity, rainfall, and wind speed can affect the incidence of malaria by impacting the changes in the duration of the parasite's life cycle and parasite behavior.

Githeko and Ndegwa (2001) focused on the East African Highlands and argued that the underlying cause of the malaria epidemic is due to the changing climatic conditions in this normally cool area. An increase in temperature has been shown to accelerate the rate of mosquito larval development and the frequency of bites on humans, as well as impacting the time it takes for the malaria parasite to mature into the mosquito stage. Increases in rainfall can create additional habitats for mosquitoes to breed, thus increasing vector populations. Githeko and Ndegwa (2001) concluded that in the past decade there has been an increase in the anomalies of mean monthly temperatures, which has a strong relationship with the number of malaria cases.

Few past studies have attempted to identify the relationship between climate variables and malaria risk in Peru. Jones et al., (2004) proposed that environmental factors are responsible for changes in the mosquito population over time. This study focused on a region in Loreto, where a higher overall mosquito population was observed from October 1996 through March 1997, which corresponds to the rainy season (Jones et al., 2004). Aramburú et al. (1999) found a positive correlation between malaria transmission periods and rainfall and higher temperatures near the Amazon River. Additionally, Aramburú et al. (1999) showed that the two precipitation peaks in 1997 occurred three months and one month before the malaria cases reached their highest levels in Loreto. These studies focused on the Loreto region but failed to take into account a long time series of climate and environmental data, which is critical to observe temporal trends.

This research goes one step further, by investigating how remote sensing and modeling products can be used to analyze trends in the annual parasite incidence by expanding on these past studies to include a longer time series, a larger study area (i.e., the whole Loreto Department), by examining a more complete set of environmental variables, and by quantifying the relationship between malaria and climate/environmental conditions. Field observations in the region are limited, as the Loreto department comprises nearly one-fourth of the landmass of Peru and has a low population density (Aramburú et al., 1999), making it difficult to conduct field collections of environmental data. Hence, remote sensing and modeling techniques are extremely valuable to obtain the necessary information of the current environmental and climate conditions of the region and to investigate the impacts of those factors on malaria transmission. In this study, we focus on analyzing the association between the annual parasite incidence at 315 health centers located in Loreto and environmental and atmospheric variables, such as temperature, humidity, soil moisture, vegetation coverage, and elevation. All of the variables are entered into a Multivariate Poisson Regression Model to study the dependence of the annual parasite incidence on these environmental conditions and identify which regions of the department are suitable for malaria transmission. Results from this study can be applied to surveillance efforts and to direct elimination strategies in higher risk regions.

2. Study area and datasets

2.1. Study area

Loreto is one of the 25 departments in Peru, located in the Northeast region of the country (Fig. 1a). Loreto comprises one fourth of Peru's land area and has a total area of approximately 348,177 km^2 (Griffing et al., 2013; Vittor et al., 2006). The region lies in the Amazon rainforest basin and has ecological characteristics of the Amazon lowlands (Aramburú et al., 1999). The region is characterized by two distinct wet and dry seasons, with the wet season going from November to May, although precipitation occurs year around. Loreto's annual average temperature is 28 °C and the region has a persistent, high relative humidity of more than 87% year around (Aramburú et al., 1999).

The Loreto region only has one major paved road with small-unpaved roads connecting villages within the region capital, the city of Iquitos. However, in practice, most of the movement in this region happens along the river networks (Abizaid, 2005; GOREL, 2006; Kvist and Nebel, 2001). As a result, a majority of the population resides in close approximation of the river (Fig. 1). In this region, the Peruvian Ministry of Health has placed more than 400 health centers, but only 315 are used as surveillance reporting units. The health centers in Loreto are nested in 8 health networks or *redes de salud* (redes, hereinafter), which are based on the boundaries of the provinces in the region. Fig. 1b-f displays maps of the health center locations, the rivers, and the boundaries of the redes. These maps show the distribution of the health centers within each of the networks (i.e., redes). Some redes have several health centers clustered in one area, while the health centers are more dispersed in other regions.

2.2. Malaria data

The malaria data used for this study are obtained from the Loreto Ministry of Health for the 2009–2013 time period. The dataset includes yearly case counts for both *Plasmodium falciparum* and *Plasmodium vivax* cases at each of the 315 health centers. The two species differ morphologically, immunologically, in their geographical distribution, and in their relapse and drug response (Tuteja, 2007). Data on the estimated population at each health center are used to determine the annual parasite incidence (API), as defined in Eq. (1):

$$API = \left(\left(\frac{number\ of\ reported\ cases\ during\ a\ time\ period}{population\ during\ time\ period} \right) * 1000 \right) \quad (1)$$

The population estimates per health center are obtained from the Loreto's Ministry of Health for the year 2009. For 2010–2013, population estimates are calculated based on linear interpolation from the 2009 population assigned to each health center and the total population estimates of the department for each year. Fig. 1b-f, which presents the API for all health centers from 2009 to 2013, shows the geographic variability in incidence rates throughout the

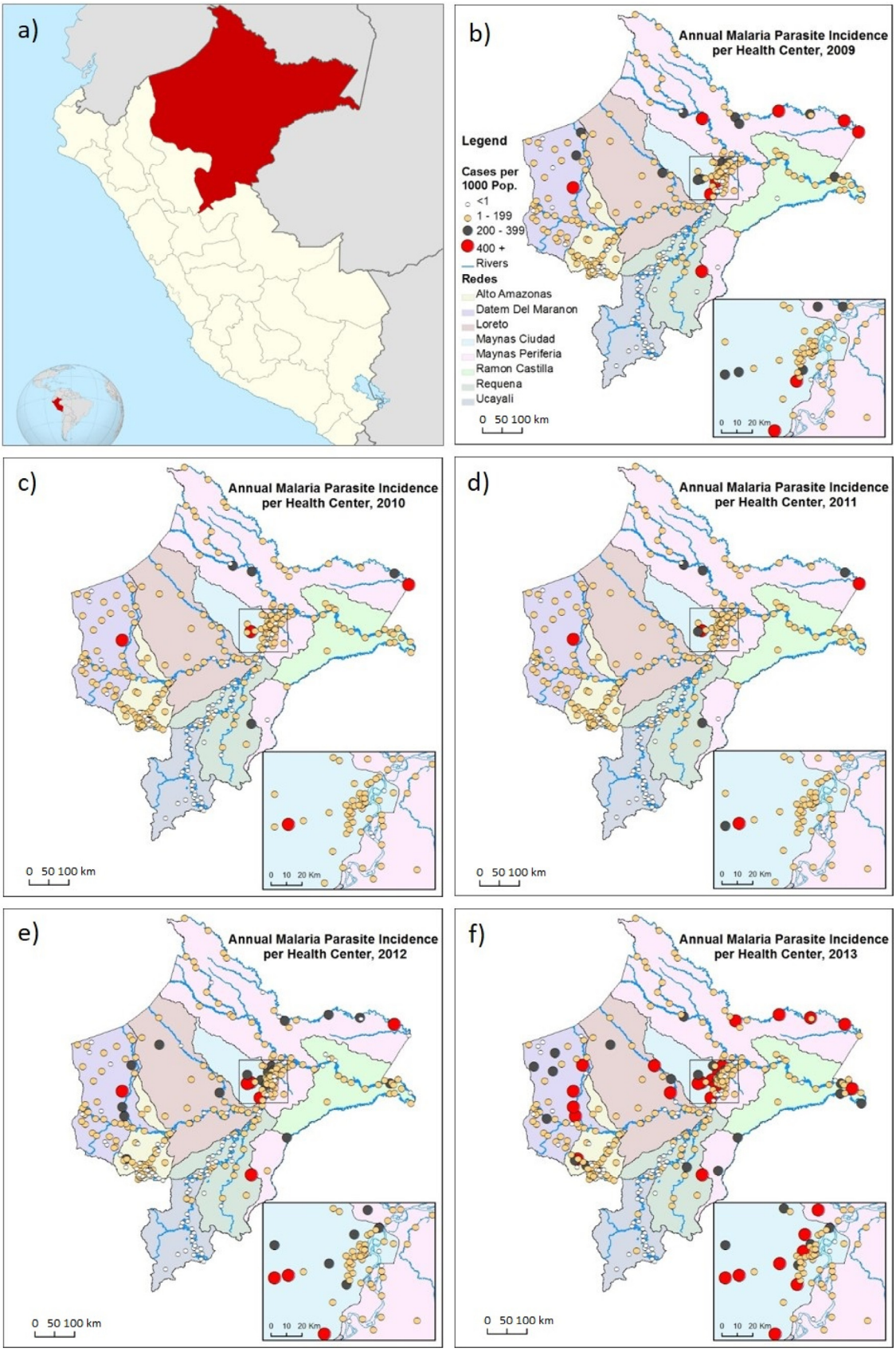

Fig. 1. (a) Location of Loreto and (b-f) Annual Malaria Parasite Incidence per Health Center for 2009–2013 with an insert map for the densely populated area.

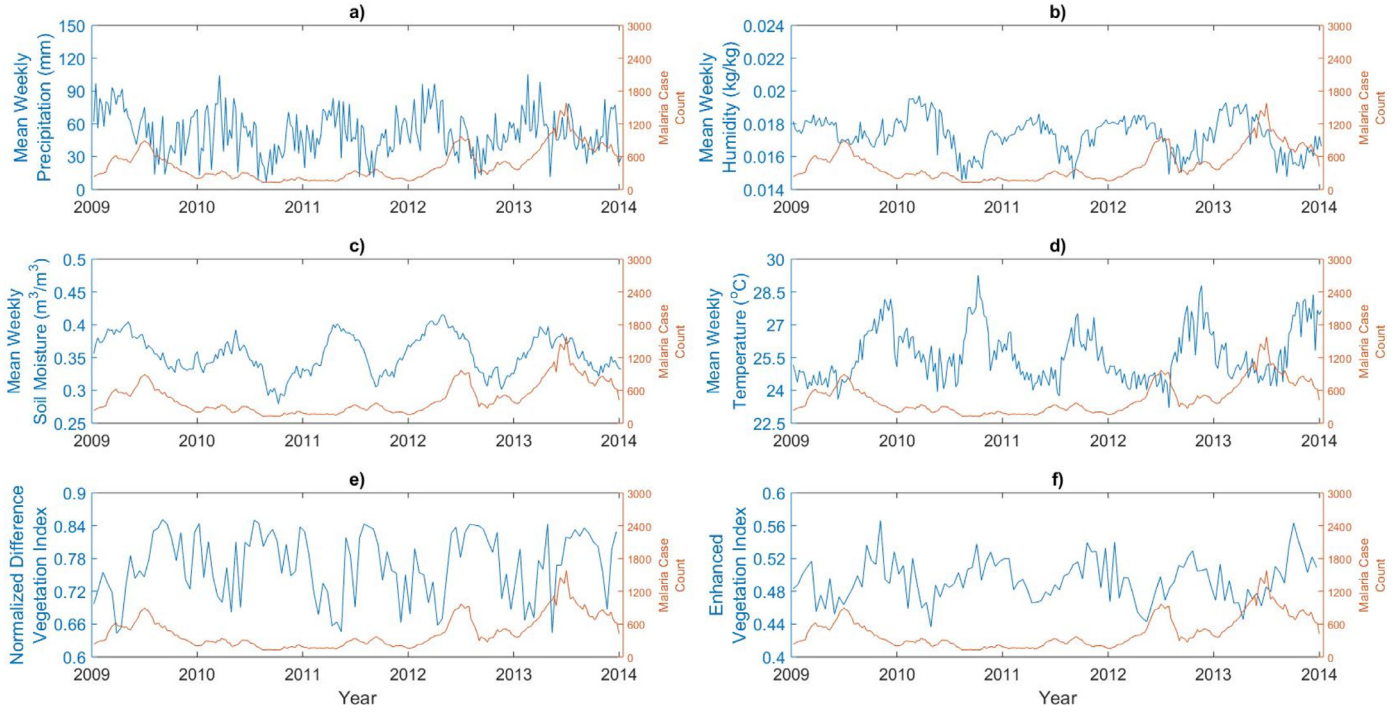

Fig. 2. Weekly time series plots for weekly malaria cases and (a) mean weekly precipitation, (b) mean weekly humidity, (c) mean weekly soil moisture, (d) mean weekly temperature, (e) mean weekly normalized difference vegetation index (NDVI), and (f) mean weekly enhanced vegetation index (EVI) for the whole Loreto Department.

redes. As depicted in the figure, more health centers had malaria incidence greater than 400 cases per 1000 people in 2013 than in previous years.

The total weekly malaria case count for the whole department is extracted for 2009–2013 from the Loreto Ministry of Health's weekly health bulletins. The results of the weekly malaria counts are presented in Fig. 2.

2.3. Climate and environmental variables

Several satellite and modeling products are used to study climate and environmental variables at each health center for 2009–2013, including outputs from the NASA MERRA (Modern-Era Retrospective analysis for Research And Applications) model, precipitation data from the Tropical Rainfall Measuring Mission (TRMM) Multisatellite Precipitation Analysis (TMPA), vegetation products from the moderate-resolution imaging spectroradiometer (MODIS) instrument, and elevation data from the Advanced Spaceborne Thermal Emission and Reflection Radiometer (ASTER) Global Elevation Model (GDEM).

2.3.1. NASA MERRA model

The MERRA model provides historical time series of the hydrological cycle variables, such as temperature, humidity, and surface pressure from 1979 to present (Reichle et al., 2011; Rienecker et al., 2011). MERRA incorporates information from remote sensing observations of the atmosphere from many modern satellites and provides estimates of surface meteorological data, e.g., precipitation, radiation, air temperature, and humidity as well as land surface variables, e.g., soil moisture and runoff. Data are available at hourly steps and at $1/2^\circ \times 2/3^\circ$ spatial resolution in latitude and longitude. The climate variables obtained from MERRA include specific humidity at 2 m above the displacement height (QV2M), temperature at 2 m above the displacement height (T2M), and soil moisture content in the top soil layer (SFMC).

2.3.2. Precipitation data

Precipitation data are obtained from the TRMM TMPA dataset (NASA, 2015). TMPA provides precipitation estimates by merging information from multiple satellite sensors and ground-based gauges (Huffman et al., 2007; Huffman et al., 2010). Specifically, this product combines the rainfall estimates of several passive microwave sensors (PMW) that are onboard Low Earth Orbit Satellites and sensors that are on board platforms of the Defense Meteorological Satellite Products (DMSP) and NOAA (Mantas et al., 2015). TMPA estimates are produced by using the PMW rain rates from each sensor through the Goddard Profiling algorithm (Gopalan et al., 2010; Kummerow et al., 2010). TMPA data are available for the 50°N–S latitude band from 1998–2014 at 3-hourly time steps and $0.25^\circ \times 0.25^\circ$ resolution (Huffman et al., 2007). The TMPA rainfall products are available in two versions: a real-time version (TMPA 3B42RT) and gauge-adjusted post real-time research version (TMPA 3B42). The main difference between the two products is the latency and the use of rain gauge data for bias adjustment (Melesse, 2011). For this study, the TMPA 3B42V7 product is selected, because of its better performance in terms of bias with respect to the real-time version (Habib et al., 2009; Maggioni et al., 2016).

2.3.3. Vegetation data

Satellite based vegetation indices are obtained from the global 16-day composite of MODIS vegetation indices that provide spatially and temporally continuous vegetation conditions. The indices include the MODIS normalized difference vegetation index (NDVI) and the Enhanced Vegetation Index (EVI), an index that provides a greater response to variations in canopy structure than NDVI (Gao et al., 2000). These data are obtained from the MOD13C1 Product at 0.05° resolution. NDVI is defined as follows:

$$\mathrm{NDVI} = \frac{\mathrm{N} - \mathrm{R}}{\mathrm{N} + \mathrm{R}} \tag{2}$$

where, N and R are the reflectance in the near-infrared (NIR) and red bands, respectively. EVI is defined as:

$$EVI = G\left(\frac{N - R}{N + C_1R - C_2B + L}\right) \quad (3)$$

where, N, R, and B are atmosphere-corrected surface reflectance in near-infrared, red, and blue bands. G is a gain factor, C1 and C2 are coefficients of the aerosol resistance term, and L is a canopy background adjustment term. The coefficients used in the MODIS EVI algorithm are, G = 2.5, C1 = 6, C2 = 7.5, and L = 1 (Huete et al., 2002).

2.3.4. Elevation data

The ASTER GDEM model provides elevation data globally at 30 m resolution. The ASTER instrument was launched onboard NASA's Terra Spacecraft and has the capability of using near infrared spectral band and nadir-viewing and backward-viewing telescopes to acquire stereo image data (Japan Space Systems, 2011; NASA, 2016). To produce the ASTER DEMs, the ASTER archive data are processed through an automated method which includes, cloud masking, stacking all cloud-screened DEMs, removing bad values, and averaging selected data to create final pixel values. The ASTER GDEM is available for land surface regions between 83° N-S in 1° × 1° tiles (Japan Space Systems, 2011).

2.3.5. Time series

Time series of weekly average precipitation, temperature, humidity, NDVI, EVI and number of malaria cases from 2009–2013 for the entire area are shown in Fig. 2. Climate and environmental factors are characterized by a strong seasonality in the region, showing the two main (dry and wet) seasons. Specifically, precipitation, humidity, and soil moisture start increasing in the last few months of the year and the peak occurs in the beginning of the year, which lines up with the wet season (November–May) in Loreto. For temperature, NDVI, and EVI, the peak occurs in the second half of each year between May and December. The peak of malaria cases occurs approximately in the middle of each year. The maximum weekly precipitation, temperature, and humidity average for the entire time period occur between 2010 and 2011, which aligns with the time when malaria cases began to increase. Appendix A presents additional weekly time series of the parameters for 2009–2013. The plots indicate that there is variability in the climate and environmental variables for the different regions of the country.

3. Methodology

3.1. Mixed effects poisson regression model

A multilevel mixed-effects Poisson regression model is used to study the relationship between Annual Parasite Incidence and atmospheric/environmental variables. This type of model is a multilevel Poisson regression that contains both fixed effects and random effects. There are many advantages of using a mixed-effect model for this type of analysis. First, mixed-effect models can be applied to continuous and non-normally distributed outcomes (e.g., Poisson distribution). Second, this family of models is robust when handling missing data, and a combination of time-invariant and time varying covariates (Gibbons et al., 2010). Mixed-effects models also allow for modeling the correlation that might exist in grouped data; therefore, the nesting of the grouped observations can be treated as random effects within the model (Buckley et al., 2003; Ren et al., 2015).

A Poisson regression model is generally utilized when the response variable is a discrete number (n = 0, 1, 2, …, N). The data available for this study can be described by a discrete variable, which represents the number of occurrences of malaria cases, i.e., the Annual Parasite Incidence. Therefore, the Poisson regression method is considered to be the most appropriate approach. In comparison to ordinary regression models, this technique has the constraint that: 1) predicted values are non-negative numbers, and 2) the mean and the variance of the errors are equal to each other. Moreover, the Poisson regression model assumes that the probability distribution of the response follows a Poisson distribution (Gardner et al., 1995; Long, 1997):

$$\Pr(y_{ij} = y|x_{ij}, u_j) = \frac{\left(\exp\left(-\mu_{ij}\right)\right)\ \mu_{ij}{}^{y}}{y!} \quad (4)$$

where $\mu_{ij} = \exp(x_{ij}\ \beta + u_j)$, j = 1, 2, . . ., m clusters (redes), with cluster j consisting of i = 1, 2, …, n_j (health centers). The responses are discrete values y_{ij} (annual parasite incidence) and the row vector x_{ij} corresponds to the covariates for the fixed effects, with the regression coefficients (fixed effects) β. The random effects are represented by u_j (STATA, 2013). In this model, the fixed effects represent the climate and environmental variables and the random effect accounts for the correlation that might exist in the redes.

The Poisson regression assumes that the logarithm of its expected value can be modeled by a linear combination of unknown parameters (Ahmed, 2014). The equation can be written as a generalized linear function as follows:

$$\log\left(\mu_{ij}\right) = \beta_0 + \beta_1 x_{ij} \ldots + \beta_n x_{ij} + u_j \quad (5)$$

where β_0 is the intercept term, β_n are the fixed effect coefficient values, and u_j is the random effects term. The coefficients can be exponentiated to determine the incidence rate ratio (IRR), which is computed as:

$$IRR = exp(\beta_n) \quad (6)$$

IRRs greater than 1 signal a positive relationship between the fixed effect and response variable, while those less than 1 signal a negative relationship. To indicate the magnitude of the effect a fixed effect has on the response variable, the IRR can be converted to a percentage value, as follows:

$$IRR(\%) = (IRR - 1) * 100 \quad (7)$$

For example, an IRR of 2 yields an IRR(%) equal to 100%, meaning that a 1 unit increase in the fixed effect would result in a 100% increase (doubling) in the response variable.

3.2. Data analysis

In this study, the mixed-effects model is implemented using a Multilevel Mixed-effects Poisson Regression in STATA 13. The model includes annual parasite incidence at each health center. The centers are clustered by redes networks to take into consideration the shared, clustered-level random effects. The atmospheric and environmental data come in gridded formats, therefore it is necessary to determine in which grid cell each of the health centers is located. To determine the conditions at each health center, the nearest neighbor value of the atmospheric/environmental data is used.

All the climate and environmental variables are transformed in an attempt to better characterize the conditions throughout the year. For example, rather than simply considering the average yearly temperature, the number of days with temperature above a certain degree is considered. Due to the fact that malaria data are available on a yearly scale, numerous transformations for the variables are considered in an attempt to test a broad range of potential representations of the environmental conditions. The full list of variable transformations is presented in Appendix B.

Each of the climate and environmental variable transformation is examined in a univariate analysis to identify the transformation

Table 1
Year malaria count and population for the whole department.

	2009	2010	2011	2012	2013
Malaria count	23,486	11,445	11,779	25,148	43,737
Population	766,169	766,578	775,321	784,113	792,935
Annual parasite incidence	30.7	14.9	15.2	32.1	55.2

Table 2
Mean and standard deviation of annual parasite incidence per red network.

	No. of Health Centers	2009		2010		2011		2012		2013	
		Mean	SD	Mean	SD	Mean	SD	Mean	SD	Mean	SD
Alto Amazonas	52	26.5	41.8	18.3	28.4	18.7	29.6	18.8	45.2	43.0	99.1
Datem Del Marañon	45	59.2	107.6	32.9	63.0	33.5	64.7	65.1	143.7	143.3	319.8
Loreto	27	52.4	78.1	21.3	28.6	21.6	29.2	43.6	85.4	80.4	140.6
Maynas ciudad	45	64.3	141.4	36.5	81.1	36.5	82.7	171.6	525.5	201.3	407.1
Maynas periferia	57	115.9	254.9	51.7	95.2	52.3	96.4	65.9	138.6	131.2	299.2
Ramon castilla	21	58.8	52.2	17.9	16.1	18.0	16.4	60.1	89.1	120.2	208.2
Requena	34	23.1	98.5	12.9	53.1	12.9	53.4	28.2	121.3	42.9	152.1
Ucayali	34	0.0	0.0	0.03	0.2	0.03	0.2	0.1	0.3	0.8	4.4

that will be included in the multivariate model. The Akaike Information Criterion (AIC), which provides a measure of the relative quality of a model for a set of data, is the chosen metric to select these transformations. The AIC is defined as:

$$AIC = -2\ln L + 2k \tag{8}$$

where lnL is the maximized log-likelihood of the model and k is the number of parameters, which in our case is the same for all the univariate models (STATA, 2013). The AIC quantifies the quality of the fitness of each univariate model and is therefore used to compare the univariate models against each other and select the best variable transformations. Given two models, the one with the smaller AIC indicates a better-fitting model (STATA, 2013).

The AIC for each of the various transformations of all variables is then calculated and, for each variable, the transformation with the lowest AIC value is included in the multivariate analysis. The forward selection is used to determine the variables for the multivariate model (Adimi et al., 2010; Ayalew et al., 2016; Lachish et al., 2013). In this approach, each variable is added to the model one at a time, starting with the one that is the most significant (i.e., lowest AIC) and assessing the effect of adding that variable on the model AIC value.

Pearson's correlation coefficients are also computed for each variable to avoid multicollinearity. Multicollinearity can inflate the variance of one of the estimated regression coefficients and produce untrustworthy model results. A coefficient value greater than 0.5 or less than −0.5 corresponds to a high degree of correlation between the two variables, so one of the two variables would be eliminated. The multivariate analysis is applied first to the annual malaria parasite incidence and then to the two types of malaria (*P. falciparum* and *P. vivax*) separately.

4. Results

4.1. Sample characteristics

The total number of malaria cases for Loreto decreased from 2009 to 2010, then began increasing afterward, reaching 43,737 cases in 2013. The yearly number of malaria cases, population, and annual parasite incidence for the entire department are presented in Table 1 for 2009–2013.

Table 2 shows the mean annual parasite incidence for the health centers in each of the eight redes, as well as the number of health centers in each. In 2013, Maynas Ciudad, Datem del Maranon, and Maynas Periferia showed the highest annual parasite incidence, whereas Ucayali recorded the lowest average annual parasite incidence among all the redes in 2013. As shown in Fig. 2, Maynad Ciudad and Maynas Periferia are located closer to the equator compared to the other redes. Datem del Maranon is located in the western region of the department near the border with Ecuador. Ucayali is located at the southernmost part of the department and the furthest away from the Equator compared to the other redes.

Another point to note in Table 2 is that the standard deviation of the annual parasite incidence is higher than the mean, which indicates high variability in annual parasite incidences among the health centers in the each of the redes.

4.2. Univariate analysis

The AIC is used to determine which variable transformation to use in the multivariate analysis (Appendix C). First, the model is created for the annual parasite incidence aggregated for species, *P. vivax* and *P. falciparum*. According to the univariate analysis, the variable transformations with the lowest AIC value, which indicate a better model fit, are the P2 (cumulative precipitation during the wet season), E2 (the elevation above 100 m), H4 (the number of days with humidity above 0.018 $kg_{vapor} \times kg_{air}^{-1}$), SM4 (the number of days with soil moisture above 0.400 m^3/m^3), T9 (the number of days with temperature above 25 °C), and NDVI (the yearly average normalized difference vegetation index).

Next, a univariate analysis is conducted for the *P. falciparum* and the *P. vivax* annual parasite incidence independently to investigate if the two types of malaria are associated with different climate and environmental conditions. For *P. falciparum* (Appendix D), the transformed variables with the lowest AIC value are the same as those for the annual parasite incidence with the exception of precipitation, where P7 (the number of days with rainfall over 15 mm) had the lowest AIC number rather than the cumulative precipitation during the wet season. For the *P. vivax* (Appendix E), the variable transformations with the lowest AIC values are the same as those for the annual parasite incidence.

4.3. Multivariate analysis

The forward selection is used to determine the variables for the multivariate model. The AIC value for each model in the forward selection is presented in Appendix F. Additionally, the correlation coefficient is calculated for each of the variables to avoid multicollinearity, similarly to the univariate analysis. Table 3 indicates

Table 3
Correlation matrix of variables used in the multivariate analysis for the total and P. vivax-annual parasite incidence model.

	T9	E2	SM4	P2	NDVI
T9	1				
E2	−0.075	1			
SM4	−0.26	-0.38	1		
P2	−0.13	0.0034	0.12	1	
NDVI	0.044	0.44	−0.32	−0.024	1

Table 4
Multivariate analysis for annual parasite incidence.

Coefficient	Estimate	95% CI	IRR–Fixed Effects
βo	−472.34	−482.66, -462.03	
β_{T9}	−0.0043	−0.0044, 0.0041	0.99
β_{E2}	0.78	0.75, 0.81	2.18
β_{SM4}	0.0021	0.0019, 0.0022	1.00
B_{P2}	0.59	0.56, 0.61	1.79
β_{NDVI}	2.13	1.83, 2.43	8.45
β_{year}	0.24	0.23, 0.24	1.26
Random effects	3.29	1.23, 8.83	

that the correlation between the variables for each multivariate model is low (i.e., between −0.075 and 0.44). Five climate and environmental factors are included in the multivariate mixed effects model based on the univariate model for the annual parasite incidence (Table 4).

Based on the results presented in Table 4, IRR can be computed for the fixed-effects variables. The IRR for T9 is 0.996 which corresponds to the 0.40% reduction in the annual parasite incidence when the number of days in the year with temperature above 25 °C increases by one day. Aramburú et al. (1999) also showed a negative correlation with temperature and malaria cases, though their study area was limited to the Iquitos region. Throughout many of the redes in Loreto, the temperature falls within optimal range (20 °C–28 °C) for mosquito development throughout much of the year with limited variation (Appendix A), which makes much of Loreto suitable for year-round malaria transmission. However, Appendix A also shows that for redes that do experience some seasonal variations in temperature, the maximum temperatures are above this optimal range, while the minimum temperatures remain within the range. As a result, the negative association in our model results is likely due to the effect of extremely high temperatures that are not conducive to mosquito development and malaria transmission.

The IRR value for E2 corresponds to a 118% increase in malaria at health centers located above 100 m. Elevation often serves as a proxy for other environmental variables and our results do not corroborate what is presented by previous studies, which showed that mosquito densities and annual parasite incidence decrease with increasing elevation (Drakeley et al., 2005; Attenborough et al., 1997; Bødke et al., 2003; Akhwale et al., 2004). However, compared to the areas these studies focused on (mainly in Africa), Loreto is characterized by a lower overall elevation and a smaller range of elevations throughout the region. Hence, the relationship in our model results is more likely due to elevation acting as a proxy for an unobserved characteristic of the region (e.g., vegetation characteristics not captured by NDVI), rather than describing the physical relationship between malaria incidence and elevation.

In terms of the SM4, a 0.2% increase in annual parasite incidence is observed when there is an increase by one day in the number of days a year with soil moisture above 0.400 m^3/m^3. This is in line with a previous study conducted over Kenya, which concluded that soil moisture better predicts the biting rates compared to rainfall (Patz et al., 1998).

Table 5
Correlation matrix of variables used in the multivariate analysis for the P. falciparum-annual parasite incidence model.

	T9	NDVI	E2	SM1	P7
T9	1				
NDVI	0.044	1			
E2	-0.075	0.44	1		
SM1	−0.4	−0.43	−0.36	1	
P7	−0.12	0.0005	−0.017	0.12	1

Table 6
Multivariate analysis for the P. falciparum-annual parasite incidence.

Coefficient	Estimate	95% CI	IRR–Fixed Effects
βo	−612.94	−639.12, -586.77	
β_{T9}	−0.0097	−0.010, -0.0094	0.99
β_{E2}	0.69	0.59, 0.76	1.97
β_{SM1}	−1.79	−2.37, 1.23	0.166
B_{P7}	0.0084	0.0069, 0.0098	1.008
β_{NDVI}	9.14	8.43, 9.84	9286.17
β_{year}	0.30	0.29, 0.32	1.35
Random effects	3.80	1.37, 10.52	

Table 7
Multivariate analysis for the P. vivax-annual parasite incidence.

Coefficient	Estimate	95% CI	IRR–Fixed Effects
βo	−442.64	−453.78, −431.49	
β_{T9}	−0.0030	−0.0031, −0.0028	0.997
β_{E2}	0.81	0.78, 0.85	2.254
β_{SM4}	0.003	0.0029, 0.0031	1.003
β_{P2}	0.63	0.60, 0.65	1.871
β_{NDVI}	0.50	0.16, 0 .83	1.642
β_{year}	0.22	0.22, 0.23	1.247
Random effects	3.11	1.16, 8.37	

Finally, the increase in P2 and the NDVI are also associated with an increased in annual parasite incidence. Since increases in NDVI and vegetation, in general, are linked to higher temperature and precipitation, this result confirms that vegetation and precipitation are fundamental factors by providing breeding sites for mosquitos (Cui et al., 2009; Hao et al., 2011).

Similar analysis is conducted for the two types of malaria present in Peru separately, i.e., *P. falciparum* and *P. vivax* annual parasite incidence. The results of the correlation coefficients and multivariate analysis for the *P. falciparum*-annual parasite incidence are shown in Tables 5 and 6.

Based on the coefficient estimates, the calculated IRR value for the *P. falciparum*-annual parasite incidence indicates that there is an increase in *P. falciparum*-annual parasite incidence associated with an increase in E2, P7, and NDVI. E7 and SM1 (yearly average soil moisture) are negatively associated with the *P. falciparum*-annual parasite incidence.

The results of the multivariate analysis and the correlation coefficients for the *P. vivax*-annual parasite incidence are shown in Tables 7 and 3, respectively.

Based on the coefficient estimates, the IRR value for the *P. vivax* annual parasite incidence indicates that there is an increase in the annual parasite incidence associated with an increase in E2, SM4, P2 and NDVI. The number of days with temperature above 25 °C is associated with a decrease in the annual parasite incidence. These results are the same as the annual parasite incidence multivariate model, which demonstrates that it is sufficient to use total cases instead of the two separate values.

However, the *P. falciparum* and *P. vivax* annual parasite incidence multivariate models present a difference in terms of which variable transformation is included in the model. For the *P. falciparum* cases, the number of days with rainfall over 15 mm is in-

cluded rather than the cumulative rainfall in the wet season. Moreover, for the *P. falciparum* annual parasite incidence model, the average yearly soil moisture is included rather than the number of days with soil moisture above 0.400 m^3/m^3.

The main difference between the two malaria types consists in the severity of the disease. *P. falciparum* can cause more severe effects because it multiplies more rapidly in the blood, whereas *P. vivax* has dormant liver stages and can relapse several months after the infecting mosquito bite (CDC, 2015). In Peru, the majority of reported cases are *P. vivax,* but *P. falciparium* transmission continues to occur. For this study, a multivariate model is created for the two malaria types and the only difference is for the *P. falciparum* annual parasite incidence model, where a different transformation is used for precipitation and soil moisture.

5. Conclusion

In this study, we analyzed annual parasite incidence data from health centers in the Loreto Department of Peru, located in the Amazon basin, to assess and quantify the association between malaria and various environmental and atmospheric factors. This region has a low population density and a large land area, making it difficult to directly collect high-resolution environmental data. Remote sensing and modeling techniques are particularly useful in remote areas like Loreto, providing temporally and spatially continuous Earth observations. This work presents a first attempt to investigate the usefulness of these techniques for better understanding and quantifying the relationship between trends in malaria incidence and a complete set of land surface and atmospheric conditions.

Ultimately, it is concluded that since the climate and environmental factors have a larger impact on the vector instead of the parasite, there is not a need to separately test the two malaria types. Specifically, higher temperature increases the number of blood meals, and number of eggs laid, which increases the number of mosquitos in a given area. Rainfall creates the sites the mosquitoes need to breed, so an increase in rainfall can result in a larger number of potential breeding locations, thereby increasing mosquito populations. Rainfall also influences vegetation growth and soil moisture, providing a moist environment conducive for mosquito breeding and longevity (Kar et al., 2014). Results from this study indicate that abundant and healthy vegetation (which corresponds to high NDVI), high precipitation amount in the wet season, elevation above 100 m, and high soil moisture content have a positive impact on annual parasite incidence in Loreto, Peru.

Malaria transmission is extremely complex. It is impacted by many factors, including gender, age, housing conditions, weather conditions, distance to standing water and occupation, among others (Ayele et al., 2012). This work solely focuses on understanding the role of climate and environmental factors, which is particularly useful, since these data are open source and available for any area of the world. Thus, similar analysis could be conducted in any other region where vector-borne disease data are available. While our study is limited by not including anthropogenic variables, further studies would benefit by incorporating other factors such as population age, occupation, access to healthcare, education, and distance from standing water. Future work could also integrate information regarding population distribution to better characterize the environmental and climate conditions the population is exposed to. However, considering the limited connectivity in Loreto (only through rivers in nearly all cases) and the hypoendemic state of malaria in this region, we believe anthropogenic-related risk factors play a less important role than the weather and environmental conditions when examining malaria incidence over broad temporal scales.

Because parasite incidence is only available on a yearly scale, a lag analysis could not be performed. In a lag analysis, malaria cases are compared with the environmental or climate conditions that occurred in a certain past period, thus incorporating time for mosquitoes to breed and for malaria symptoms to show. Given the time scale of our incidence data, we evaluated numerous transformations of the climate and environmental variables in an effort to find those having the strongest relationship with malaria incidence in this region. Although this approach was exploratory and created temporal mismatches among the variables, these transformations remained grounded to established relationships among the phenomena and were synchronized with the temporal range of the incidence data. While our models identified vegetation, precipitation, elevation, and soil moisture as important predictors of malaria incidence, the temporal mismatch and ecological nature of our analysis do not allow for us to establish causality based on our results.

This work represents an important first step to understanding the dynamics between malaria incidence and the climate and environmental conditions in the Loreto region. Specifically, we focused on understanding the explanatory factors of malaria, rather than predicting incidence rates, which would necessitate a much different overall modeling approach. Despite the highlighted limitations, results from this study have the potential of being useful for healthcare workers in malaria endemic areas and being integrated within a malaria elimination plan by creating risk maps. Results from this and future studies will inform efforts to develop a global framework for predicting and monitoring the spread of malaria, especially in relation to climate and environmental variables and their change over time.

Acknowledgments

The authors would also like to thank the Loreto Ministry of Health for providing the malaria dataset, NASA Precipitation Processing System (PPS) for the TMPA 3B42 data, the Global Modeling and Assimilation Office (GMAO) and the GES DISC for the dissemination of MERRA.

Appendix A: Weekly time series for each weather parameter per red for *2009–2013*

Precipitation

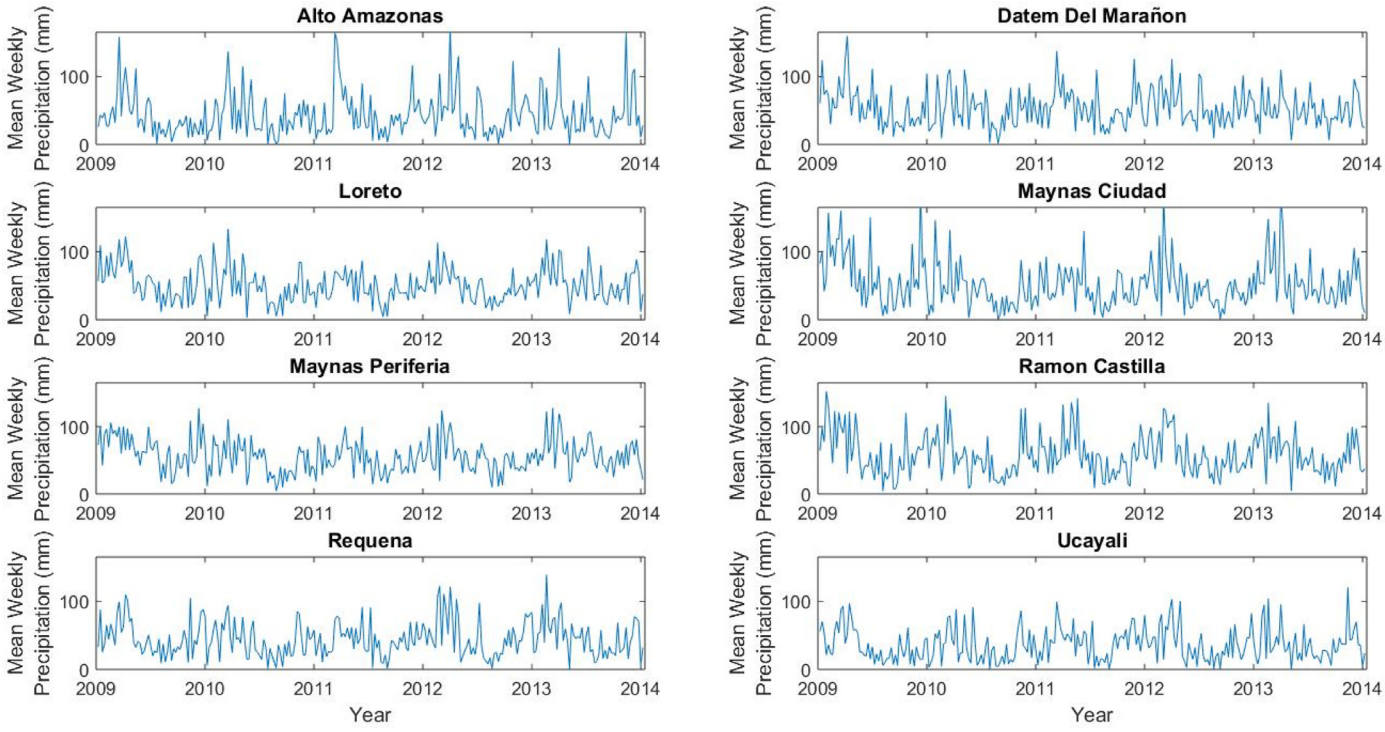

Temperature

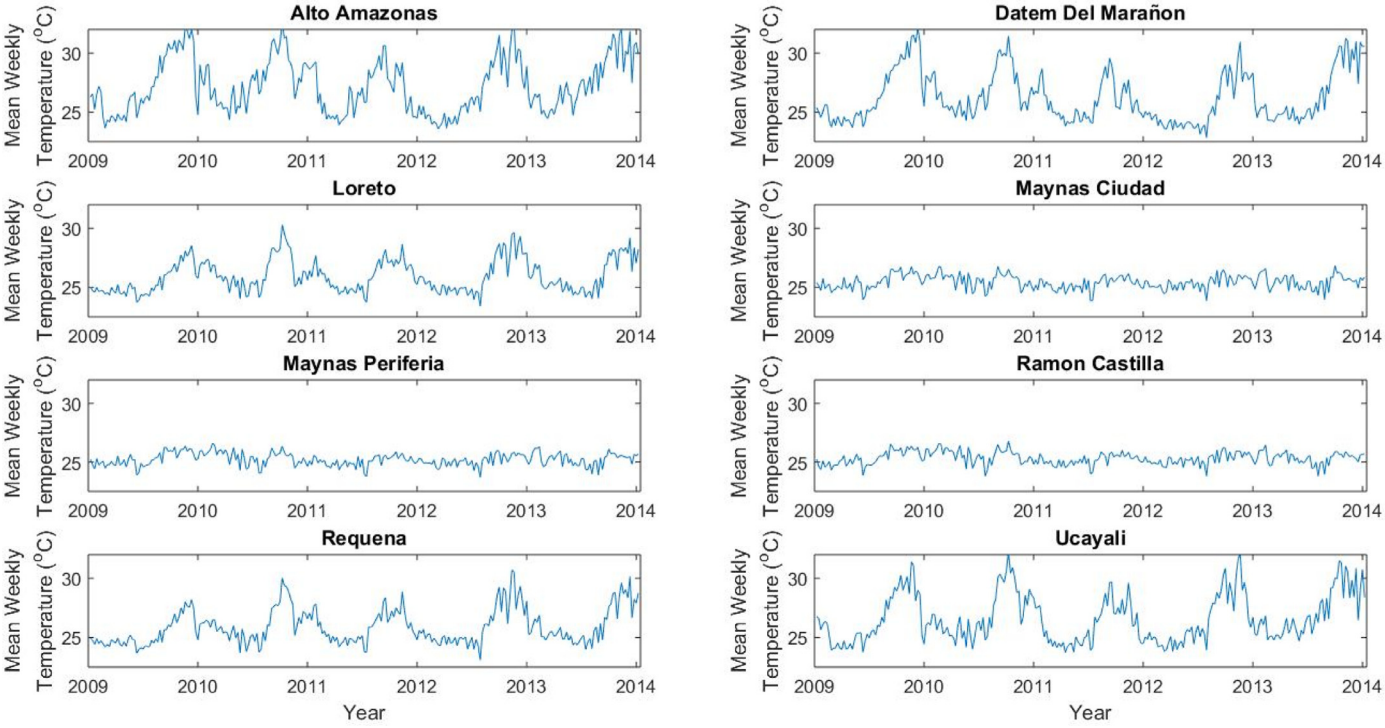

Humidity

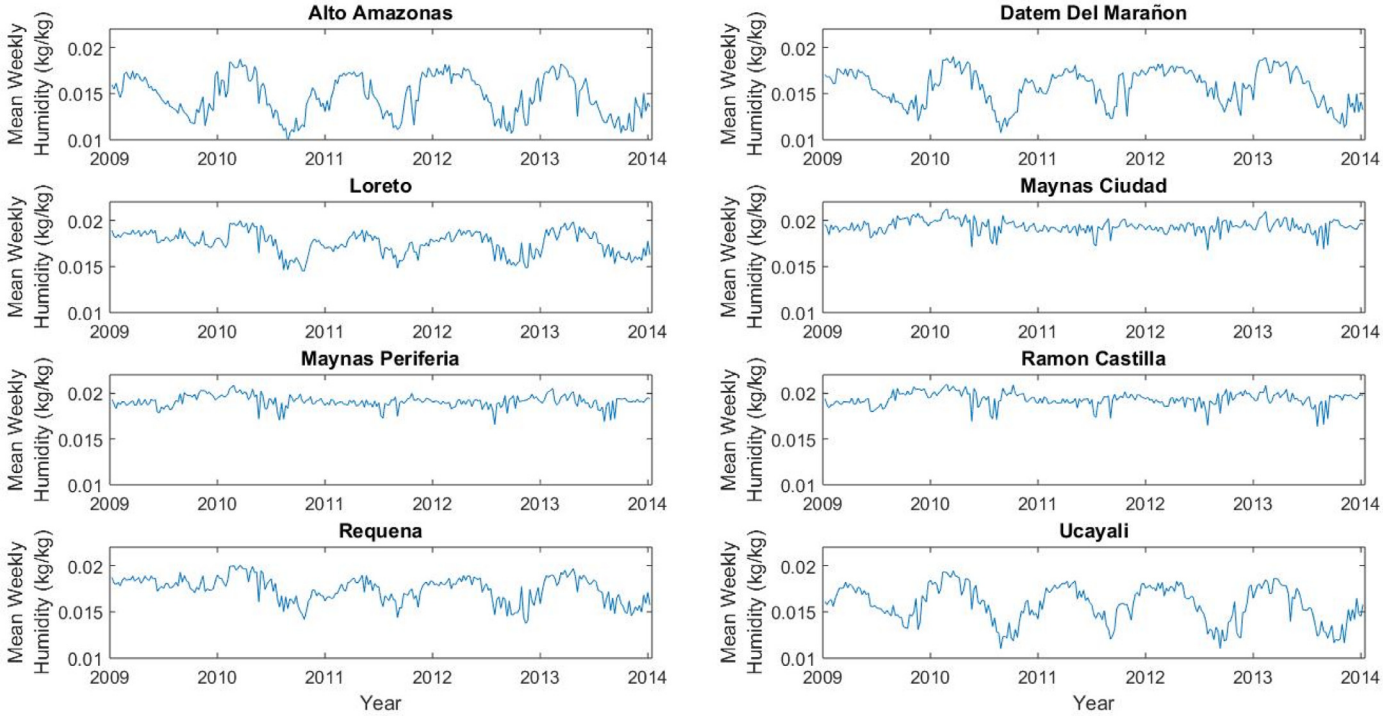

Soil Moisture

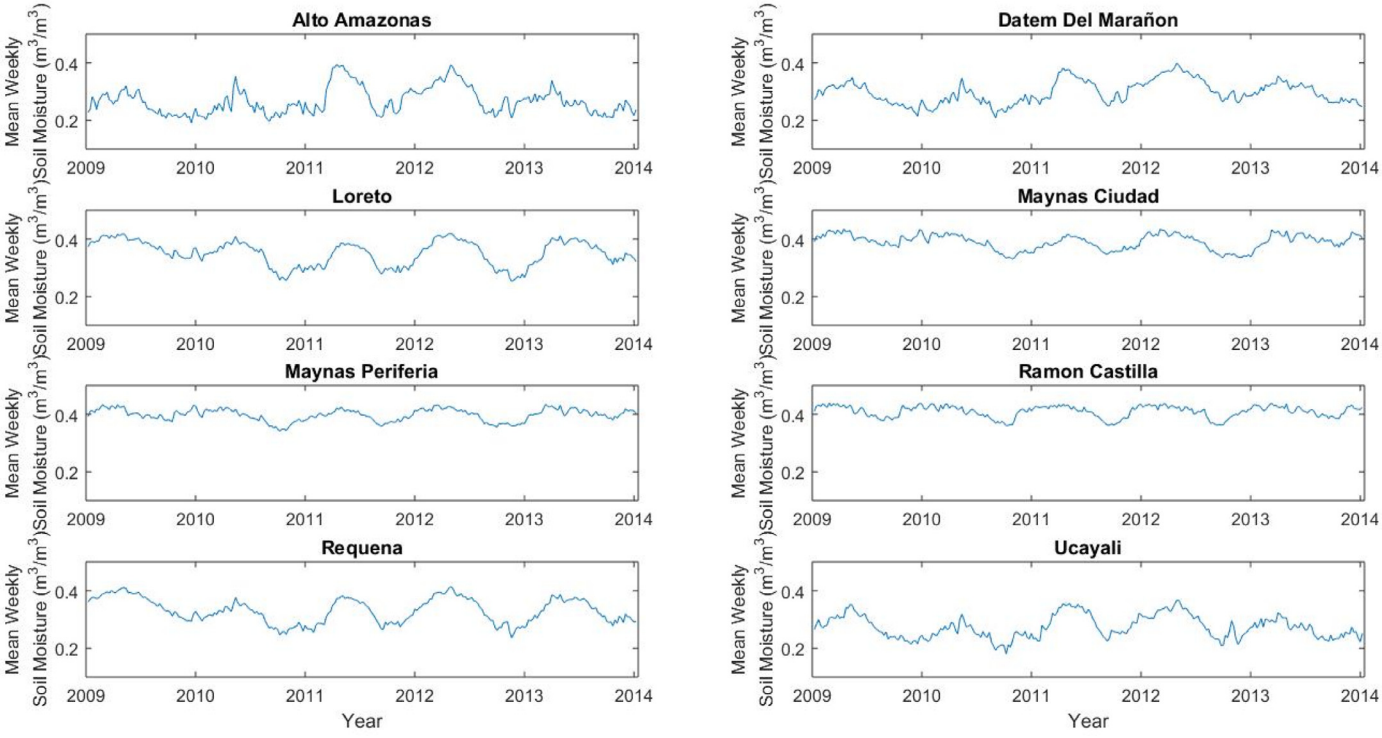

NDVI

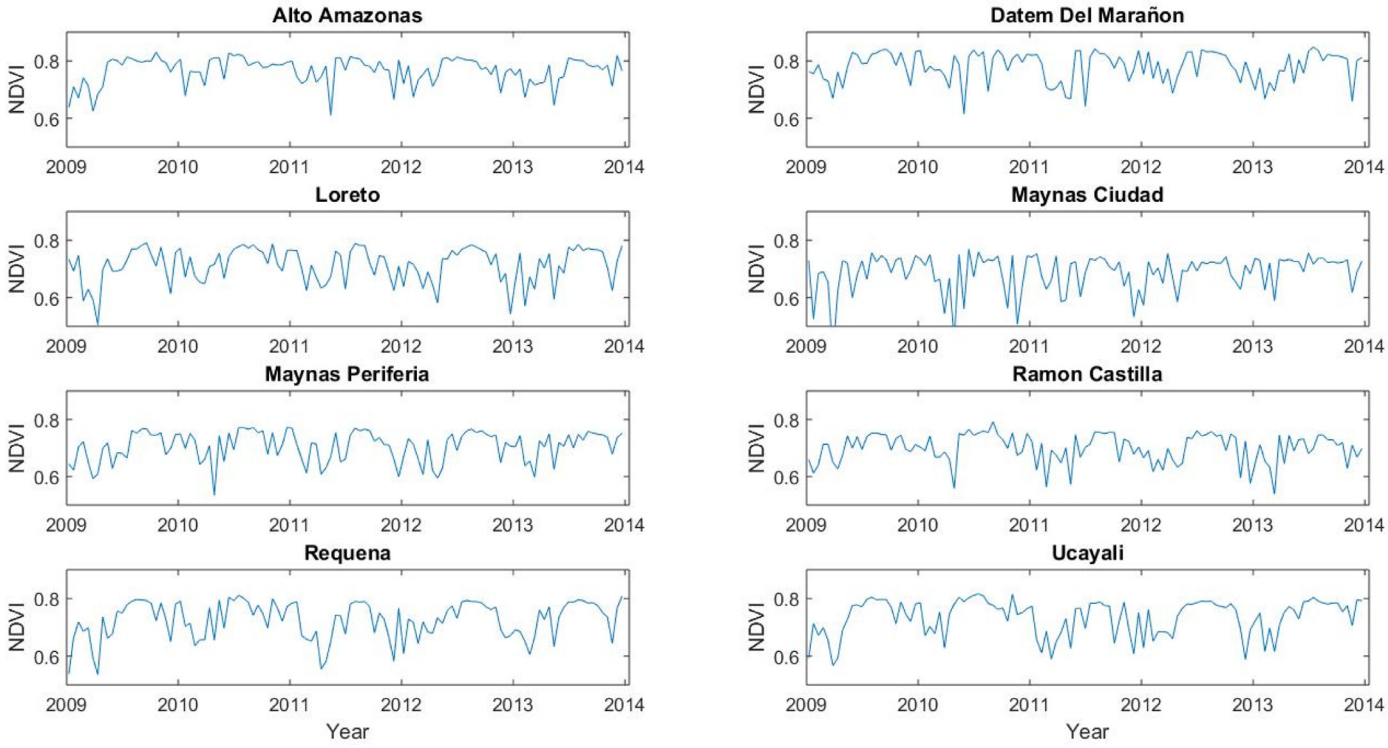
Alto Amazonas
Datem Del Marañon
Loreto
Maynas Ciudad
Maynas Periferia
Ramon Castilla
Requena
Ucayali
NDVI
0.8
0.6
2009
2010
2011
2012
2013
2014
Year

EVI

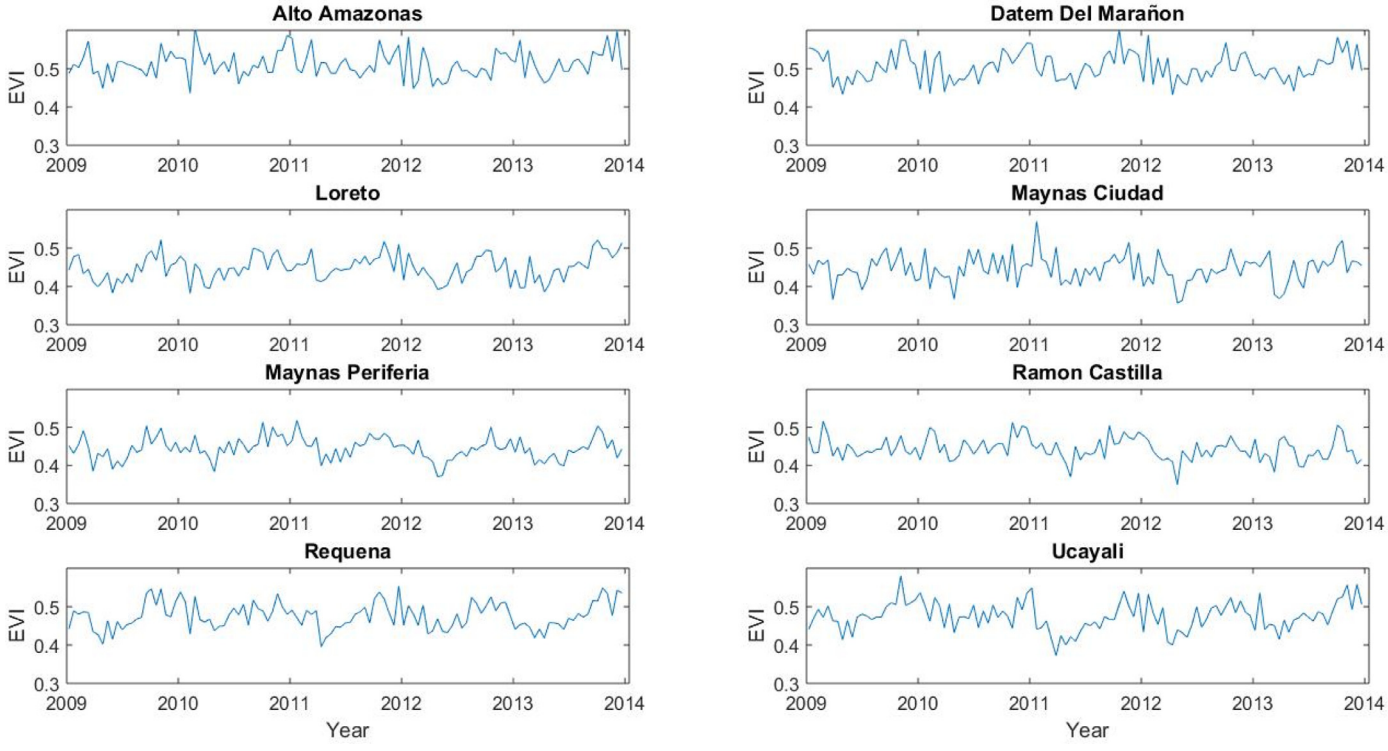
Alto Amazonas
Datem Del Marañon
Loreto
Maynas Ciudad
Maynas Periferia
Ramon Castilla
Requena
Ucayali
EVI
0.5
0.4
0.3
2009
2010
2011
2012
2013
2014
Year

Appendix B. Acronyms

	Precipitation
$\mathbf{P_1}$	Cumulative in the whole year (m)
$\mathbf{P_2}$	Cumulative in the wet season (m)
$\mathbf{P_3}$	Cumulative in the dry season (m)
$\mathbf{P_4}$	Number of days without rainfall
$\mathbf{P_5}$	Number of days with rainfall over 10 mm
$\mathbf{P_6}$	Number of days with rainfall over 12 mm
$\mathbf{P_7}$	Number of days with rainfall over 15 mm
$\mathbf{P_8}$	Number of months with rainfall over 60 mm
	Temperature
$\mathbf{T_1}$	Average daily temperature in the whole year (°C)
$\mathbf{T_2}$	Average daily temperature in the wet season (°C)
$\mathbf{T_3}$	Average daily temperature in the dry season (°C)
$\mathbf{T_4}$	Mean maximal temperature in the whole year (°C)
$\mathbf{T_5}$	Mean maximal temperature in the wet season (°C)
$\mathbf{T_6}$	Mean minimal temperature in the whole year (°C)
$\mathbf{T_7}$	Mean minimal temperature in the dry season (°C)
$\mathbf{T_8}$	Number of days with temperature above 30 °C
$\mathbf{T_9}$	Number of days with temperature above 25 °C
$\mathbf{T_{10}}$	Number of days with temperature under 20 °C
$\mathbf{T_{11}}$	Number of days with temperature under 15 °C
$\mathbf{T_{12}}$	Average temperature at night (6pm/6am) in the wet season (°C)
$\mathbf{T_{13}}$	Average temperature at night (6pm/6am) in the dry season (°C)
	Humidity
$\mathbf{H_1}$	Average daily humidity in the whole year (kg vapor × $kgair^{-1}$)
$\mathbf{H_2}$	Average daily humidity in the wet season (kg vapor × $kgair^{-1}$)
$\mathbf{H_3}$	Average daily humidity in the dry season (kg vapor × $kgair^{-1}$)
$\mathbf{H_4}$	Number of days with humidity above 0.018 kg vapor × $kgair^{-1}$
$\mathbf{H_5}$	Number of days with humidity under 0.016 kg vapor × $kgair^{-1}$
$\mathbf{H_6}$	Number of days with humidity under 0.014 kg vapor × $kgair^{-1}$
	Soil moisture
SM1	Average daily soil moisture in the whole year (m^3*m^{-3})
$\mathbf{SM_2}$	Average daily soil moisture in the wet season (m^3*m^{-3})
$\mathbf{SM_3}$	Average daily soil moisture in the dry season (m^3*m^{-3})
$\mathbf{SM_4}$	Number of days with soil moisture above 0.400 m^3*m^{-3}
$\mathbf{SM_5}$	Number of days with soil moisture under 0.300 m^3*m^{-3}
	Vegetation index
EVI	Average annual enhanced vegetation index
NDVI	Average annual normalized difference vegetation Index
	Elevation
$\mathbf{E_1}$	Elevation (m)
$\mathbf{E_2}$	Elevation above 100 m
$\mathbf{E_3}$	Elevation above 150 m
$\mathbf{E_4}$	Elevation above 200 m

Appendix C: *Univariate analysis for the annual parasite incidence*

Parameter	Incidence rate ratio	(95% CI)	AIC
$\mathbf{P_1}$	1.555	1.532, 1.578	219,412
$\mathbf{P_2}$	2.094	2.049, 2.138	218,222
$\mathbf{P_3}$	1.498	1.452, 1.544	222,214
$\mathbf{P_4}$	0.993	0.994, 0.993	220,441
$\mathbf{P_5}$	1.013	1.012, 1.013	220,110
$\mathbf{P_6}$	1.014	1.014, 1.015	220,089
$\mathbf{P_7}$	1.017	1.017, 1.018	219,707
$\mathbf{P_8}$	1.062	1.059, 1.066	221,169
$\mathbf{T_1}$	0.683	0.674, 0.692	219,411
$\mathbf{T_2}$	1.04	1.034, 1.060	222,804
$\mathbf{T_3}$	0.688	0.681, 0.694	216,885
$\mathbf{T_4}$	0.929	0.926, 0.933	221,103
$\mathbf{T_5}$	0.900	0.897, 0.905	220,892
$\mathbf{T_6}$	0.922	0.912, 0.933	222,676
$\mathbf{T_7}$	0.821	0.813, 0.829	221,505
$\mathbf{T_8}$	0.998	0.997, 0.999	222,799
$\mathbf{T_9}$	0.994	0.994, 0.994	215,851
$\mathbf{T_{10}}$	1.983	1.815, 2.167	222,701

(*continued on next page*)

Parameter	Incidence rate ratio	(95% CI)	AIC
T_{11}	1		222,857
T_{12}	0.812	0.806, 0.819	220,360
T_{13}	0.887	0.883, 0.891	219,256
H_1	4.18e-63	1.11e-67, 1.58e-58	222,143
H_2	1.5e-113	8.3e-119, 2.5e-108	221,067
H_3	6.85e-25	3.48e-28, 1.35e-21	222,652
H_4	0.995	0.995, 0.996	220,335
H_5	0.997	0.997, 0.998	222,362
H_6	0.996	0.995, 0.996	222,121
SM_1	885	706, 1109	219,376
SM_2	279	221, 353	220,638
SM_3	803	656, 984	218,650
SM_4	1.003	1.003, 1.004	218,015
SM_5	0.998	0.998, 0.998	221,520
EVI	1.246	0.886, 1.754	222,858
NDVI	1485	1148, 1922	219,755
E_1	1.000	0.999, 1.000	222,858
E_2	2.730	2.652, 2.799	216,387
E_3	1.011	0.991, 1.032	222,858
E_4	0.568	0.552, 0.584	221,168

Appendix D: *Univariate analysis for P. falciparum annual parasite incidence*

Parameter	Incidence rate ratio	(95% CI)	AIC
P_1	1.271	1.226, 1.319	50,210
P_2	1.505	1.426, 1.587	50,153
P_3	1.250	1.158, 1.350	50,343
P_4	1.001	1.000, 1.002	50,353
P_5	1.006	1.005, 1.007	50,258
P_6	1.009	1.008, 1.010	50,176
P_7	1.011	1.010, 1.012	50,143
P_8	1.052	1.045, 1.059	50,182
T_1	0.516	0.502, 0.530	48,190
T_2	0.789	0.769, 0.810	50,059
T_3	0.546	0.534, 0.558	47,360
T_4	0.982	0.975, 0.990	50,358
T_5	0.945	0.934, 0.955	50,274
T_6	0.794	0.773, 0.815	50,101
T_7	0.799	0.779, 0.819	50,082
T_8	0.989	0.988, 0.990	49,837
T_9	0.989	0.989, 0.989	46,616
T_{10}	2.72	2.343, 3.166	50,273
T_{11}	1		50,373
T_{12}	0.852	0.836, 0.869	50,119
T_{13}	0.969	0.960, 0.978	50,332
H_1	3.7e-140	6.1e-151, 2.3e-129	49,720
H_2	2.4e-210	1.0e-222, 5.4e-198	49,243
H_3	5.66e-70	1.03e-77, 3.11e-62	50,062
H_4	0.991	0.990, 0.991	48,306
H_5	0.998	0.997, 0.998	50,321
H_6	0.994	0.994, 0.995	50,088
SM_1	132	79, 220	50,029
SM_2	10.2	5.97, 17.6	50,305
SM_3	409	258, 648	49,719
SM_4	1.000	1.00, 1.00	50,369
SM_5	0.997	0.997, 0.998	50,038
EVI	65	28.9, 148.7	50,274
NDVI	1217	648,592, 2,285,897	48,441
E_1	1.000	1.000, 1.000	50,357
E_2	3.657	3.38, 3.95	48,988
E_3	1.190	1.13, 1.24	50,319
E_4	0.456	0.426, 0.488	49,789

Appendix E: *Univariate analysis for P. vivax cases annual parasite incidence*

Parameter	Incidence rate ratio	(95% CI)	AIC
P_1	1.611	1.589, 1.641	184,574
P_2	2.220	2.175, 2.271	183,398
P_3	1.540	1.497, 1.601	187,353
P_4	0.991	0.990, 0.99	184,823
P_5	1.014	1.013, 1.014	185,230
P_6	1.015	1.014, 1.015	185,358
P_7	1.018	1.017, 1.019	185,006
P_8	1.064	1.061, 1.067	186,487
T_1	0.734	0.724, 0.745	186,183
T_2	1.126	1.110, 1.141	187,698
T_3	0.726	0.718, 0.734	184,456
T_4	0.918	0.915, 0.922	186,029
T_5	0.891	0.886, 0.896	186,025
T_6	0.953	0.941, 0.965	187,932
T_7	0.825	0.816, 0.835	186,922
T_8	1.000	1.000, 1.001	187,978
T_9	0.994	0.994, 0.995	183,856
T_{10}	1.772	1.587, 1.977	187,910
T_{11}	1		187,984
T_{12}	0.804	0.796, 0.811	185,704
T_{13}	0.869	0.865, 0.873	184,008
H_1	1.22e-45	1.05e-50, 1.42e-40	187,683
H_2	3.08e-91	4.82e-97, 1.97e-85	187,047
H_3	1.65e-14	3.71e-18, 7.33e-11	187,931
H_4	0.996	0.996, 0.997	186,813
H_5	0.997	0.997, 0.998	187,531
H_6	0.996	0.996, 0.996	187,491
SM_1	1404	1092, 1806	184,779
SM_2	601	464, 779	185,656
SM_3	954	761, 1195	184,410
SM_4	1.004	1.004, 1.004	182,365
SM_5	0.998	0.998, 0.998	186,975
EVI	0.533	0.365, 0.776	187,975
NDVI	396	298, 526	186,259
E_1	0.999	0.999, 1.000	187,985
E_2	2.607	2.533, 2.683	182,838
E_3	0.976	0.955, 0.998	187,981
E_4	0.597	0.579, 0.616	186,838

Appendix F: *AIC using the Forward selection method for the Multivariate Models*

P. falciparum and P. vivax

Model	AIC
Empty	222,857
T9	215,851
T9 + E2	210,815
T9 + E2 + SM4	208,848
T9 + E2 + SM4 + P2	205,998
T9 + E2 + SM4 + P2 + NDVI	**205,806**
T9 + E2 + SM4 + P2 + NDVI + H4 *	204,769
T9 + E2 + P2 + H4 +	206,882

* H4 was correlated with NDVI and SM4

P. falciparum

Model	AIC
Empty	50,373
T9	46,616
T9 + H4	45,878
T9 + H4 + NDVI *	44,927
T9 + NDVI	45,266
T9 + NDVI + E2	44,996
T9 + H4 + E2	45,166
T9 + NDVI + E2 + SM3	44,992
T9 + NDVI + E2 + SM3 + P7 **	44,891
T9 + NDVI + E2 + SM1 + P7	**44,854**

* H4 and NDVI were correlated

** Confidence interval for SM3 included zero so SM1 was used

P. vivax

Model	AIC
Empty	187,984
SM4	182,365
SM4 + E2	177,953
SM4 + E2 + P2	17,510
SM4 + E2 + P2 + T9	173,839
SM4 + E2 + P2 + T9 + NDVI	**173,832**
SM4 + E2 + P2 + T9 + NDVI + H4 *	173,004
E2 + P2 + T9 + H4	175,922

* H4 was correlated with SM4 and NDVI

References

Abizaid, C., 2005. Geographical field note an anthropogenic meander cutoff along the Ucayali river, Peruvian Amazon. Geog. Rev. 95 (1), 122–135.

Adimi, F., Soebiyanto, R.P., Safi, N., Kiang, R., 2010. Towards malaria risk prediction in Afghanistan using remote sensing. Malar. J. 9 (1), 125. https://doi.org/10.1186/1475-2875-9-125.

Ahmed, S.E., 2014. Penalty, Shrinkage and Pretest Strategies. Springer International Publishing, Cham Retrieved from http://link.springer.com/10.1007/978-3-319-03149-1 .

Akhwale, W.S., Lum, J.K., Kaneko, A., Eto, H., Obonyo, C., Björkman, A., Kobayakawa, T., 2004. Anemia and malaria at different altitudes in the western highlands of Kenya. Acta Trop. 91 (2), 167–175. https://doi.org/10.1016/j.actatropica.2004.02.010(.

Aramburú Guarda, J., Ramal Asayag, C., Witzig, R., 1999. Malaria reemergence in the Peruvian Amazon region. Emerging Infect. Dis.s 5 (2), 209–215. https://doi.org/10.3201/eid0502.990204.

Attenborough, R.D., Burkot, T.R., Gardner, D.S., 1997. Altitude and the risk of bites from mosquitoes infected with malaria and filariasis among the Mianmin people of Papua New Guinea. Trans. R. Soc. Trop. Med. Hygiene 91 (1), 8–10. https://doi.org/10.1016/S0035-9203(97)90373-4.

Ayalew, S., Mamo, H., Animut, A., Erko, B., 2016. Assessment of current malaria status in light of the ongoing control interventions, socio-demographic and environmental variables in jiga area, northwest ethiopia. PLoS ONE 11 (1), e0146214. https://doi.org/10.1371/journal.pone.0146214.

Ayele, D.G., Zewotir, T.T., Mwambi, H.G., 2012. Prevalence and risk factors of malaria in Ethiopia. Malar. J. 11, 195. https://doi.org/10.1186/1475-2875-11-195.

Bautista, C.T., Chan, A.S.T., Ryan, J.R., Calampa, C., Roper, M.H., Hightower, A.W., Magill, A.J., 2006. Epidemiology and spatial analysis of malaria in the Northern Peruvian Amazon. Am. J. Trop. Med. Hyg. 75 (6), 1216–1222.

Bødker, R., Akida, J., Shayo, D., Kisinza, W., Msangeni, H.A., Pedersen, E.M., Lindsay, S.W., 2003. Relationship between altitude and intensity of malaria transmission in the Usambara Mountains, Tanzania. J. Med. Entomol. 40 (5), 706–717. https://doi.org/10.1603/0022-2585-40.5.706.

Buckley, Y.M., Briese, D.T., Rees, M., 2003. Demography and management of the invasive plant species Hypericum perforatum. I. Using multi-level mixed-effects models for characterizing growth, survival and fecundity in a long-term data set. J. Applied Ecology 40 (3), 481–493. https://doi.org/10.1046/j.1365-2664.2003.00821.x.

Centers for Disease Control and Prevention CDC, CDC - malaria - about malaria - biology - malaria parasites, 2015, Retrieved April 15, 2016, from http://www.cdc.gov/malaria/about/biology/parasites.html.

Chuquiyauri, R., Paredes, M., Peñataro, P., Torres, S., Marin, S., Tenorio, A., Brouwer, K.C., Abeles, S., Llanos-Cuentas, A., Gilman, R.H., Kosek, M., Vinetz, J.M., 2012. Socio-demographics and the development of malaria elimination strategies in the low transmission setting. Acta Trop. 121 (3), 292–302. https://doi.org/10.1016/j.actatropica.2011.11.003.

Cui, X., Parker, D.J., Morse, A.P., 2009. The drying out of soil moisture following rainfall in a numerical weather prediction model and implications for malaria prediction in West Africa. Weather Forecasting 24 (6), 1549–1557. https://doi.org/10.1175/2009WAF2222240.1.

Drakeley, C.J., Carneiro, I., Reyburn, H., Malima, R., Lusingu, J.P.A., Cox, J., Riley, E.M., 2005. Altitude-dependent and -independent variations in plasmodium falciparum prevalence in Northeastern Tanzania. J. Infect. Dis. 191 (10), 1589–1598. https://doi.org/10.1086/429669.

Gardner, W., Mulvey, E.P., Shaw, E.C., 1995. Regression analyses of counts and rates: poisson, overdispersed poisson, and negative binomial models. Psychol. Bull. 118 (3), 392–404.

Gao, X., Huete, A.R., Ni, W., Miura, T., 2000. Optical–biophysical relationships of vegetation spectra without background contamination. Remote Sens. Environ. 74 (3), 609–620. https://doi.org/10.1016/S0034-4257(00)00150-4.

Gibbons, R.D., Hedeker, D., DuToit, S., 2010. Advances in Analysis of Longitudinal Data. In: NolenHoeksema, S., Cannon, T.D., Widiger, T. (Eds.). In: Annual Review of Clinical Psychology, Vol 6. Annual Reviews, Palo Alto, pp. 79–107.

Griffing, S.M., Gamboa, D., Udhayakumar, V., 2013. The history of 20th century malaria control in Peru. Malar. J. 12, 303. https://doi.org/10.1186/1475-2875-12-303.

Githeko, A.K., Ndegwa, W., 2001. Predicting malaria epidemics in the Kenyan highlands using climate data: a tool for decision makers. Global Change Hum. Health 2, 54–63.

Gopalan, K., Wang, N.-Y., Ferraro, R., Liu, C., 2010. Status of the TRMM 2A12 land precipitation algorithm. J. Atmos. Oceanic Technol. 27 (8), 1343–1354. https://doi.org/10.1175/2010JTECHA1454.1.

GOREL, 2006. Mapa de la hidrografía principal y secundaria, departamento de Loreto. Gobierno regional de Loreto, Iquitos.

Habib, E., Henschke, A., Adler, R.F., 2009. Evaluation of TMPA satellite-based research and real-time rainfall estimates during six tropical-related heavy rainfall events over Louisiana, USA. Atmos. Res. 94 (3), 373–388. https://doi.org/10.1016/j.atmosres.2009.06.015.

Hao, F., Zhang, X., Ouyang, W., Skidmore, A.K., Toxopeus, A.G., 2011. Vegetation NDVI linked to temperature and precipitation in the upper catchments of yellow river. Environ. Model. Assess. 17 (4), 389–398. https://doi.org/10.1007/s10666-011-9297-8.

Herrera, S., Quiñones, M.L., Quintero, J.P., Corredor, V., Fuller, D.O., Mateus, J.C., Calzada, J.E., Gutierrez, J.B., Llanos, A., Soto, E., Menendez, C., Wu, T., Alondo, P., Carrasquilla, G., Galinski, M., Beier, J.C., Arevalo-Herrera, M., 2012. Prospects for malaria elimination in non-Amazonian regions of Latin America. Acta Trop. 121 (3), 315–323. https://doi.org/10.1016/j.actatropica.2011.06.018.

Hiwat, H., Bretas, G., 2011. Ecology of Anopheles darlingi root with respect to vector importance: a review. Parasites Vectors 4, 177. https://doi.org/10.1186/1756-3305-4-177.

Huete, A., Didan, K., Miura, T., Rodriguez, E.., Gao, X., Ferreira, L., 2002. Overview of the radiometric and biophysical performance of the MODIS vegetation indices. Remote Sens. Environ. 83 (1–2), 195–213. https://doi.org/10.1016/S0034-4257(02)00096-2.

Huffman, G.J., Bolvin, D.T., Nelkin, E.J., Wolff, D.B., Adler, R.F., Gu, G., Stocker, E.F., 2007. The TRMM multisatellite precipitation analysis (tmpa): quasi-global, multiyear, combined-sensor precipitation estimates at fine scales. J. Hydrometeor. 8 (1), 38–55. https://doi.org/10.1175/JHM560.1.

Huffman, G.J., Adler, R.F., Bolvin, D.T., Nelkin, E.J., 2010. The TRMM Multi-Satellite Precipitation Analysis (TMPA). In: Gebremichael, M., Hossain, F. (Eds.), Satellite Rainfall Applications for Surface Hydrology. Springer, Netherlands, pp. 3–22. Retrieved from http://link.springer.com/chapter/10.1007/978-90-481-2915-7_1.

Japan Space Systems, Data specification, 2011, Retrieved April 2, 2016, from http://www.jspacesystems.or.jp/ersdac/GDEM/E/4.html.

Jones, J.W., Turell, M.J., Sardelis, M.R., Watts, D.M., Coleman, R.E., Fernandez, R., Carbajal, F., Pecor, J.E., Calampa, C., Klein, T.A., 2004. Seasonal distribution, biology, and human attraction patterns of culicine mosquitoes (Diptera: Culicidae) in a forest near Puerto Almendras, Iquitos. J.Med. Entomol. 41 (3), 349–360.

Kar, N.P., Kumar, A., Singh, O.P., Carlton, J.M., Nanda, N., 2014. A review of malaria transmission dynamics in forest ecosystems. Parasites Vectors 7 (1), 1–12. https://doi.org/10.1186/1756-3305-7-265.

Kummerow, C.D., Ringerud, S., Crook, J., Randel, D., Berg, W., 2010. An observationally generated a priori database for microwave rainfall retrievals. J. Atmos. Oceanic Technol. 28 (2), 113–130. https://doi.org/10.1175/2010JTECHA1468.1.

Kvist, L.P., Nebel, G., 2001. A review of Peruvian flood plain forests: ecosystems, inhabitants and resource use. For. Ecol. Manage. 150 (1-2), 3–26.

Lachish, S., Knowles, S.C.L., Alves, R., Sepil, I., Davies, A., Lee, S., Wood, M.J., Sheldon, B.C., 2013. Spatial determinants of infection risk in a multi-species avian malaria system. Ecography 36 (5), 587–598. https://doi.org/10.1111/j.1600-0587.2012.07801.x.

Long, J.S., 1997. Regression Models for Categorical and Limited Dependent Variables, Chapter 8. Sage Publications, Thousand Oaks, CA.

Maggioni, V., Meyers, P.C., Robinson, M.D., 2016. A review of merged high-resolution satellite precipitation product accuracy during the Tropical Rainfall Measuring Mission (TRMM) era. J. Hydrometeorol. 17 (4), 1101–1117. https://doi.org/10.1175/JHM-d-15-0190.1.

Mantas, V.M., Liu, Z., Caro, C., Pereira, A.J.S.C., 2015. Validation of TRMM multisatellite precipitation analysis (TMPA) products in the Peruvian Andes. Atmos. Res. 163, 132–145. https://doi.org/10.1016/j.atmosres.2014.11.012.

Melesse, A.M., 2011. Nile River Basin: Hydrology, Climate and Water Use. Springer Science & Business Media.

NASA, 2015. TRMM data downloads | precipitation measurement missions Retrieved April 9, 2016, from http://pmm.nasa.gov/data-access/downloads/trmm.

NASA, 2016. Reverb | ECHO Retrieved April 9, 2016, from http://reverb.echo.nasa.gov/reverb/#utf8=%E2%9C%93&spatial_map=satellite&spatial_type=rectangle.

PAMAFRO [Report of Results No 10], 2010, Retrieved September 5, 2016, from http://www.orasconhu.org/sites/default/files/1ReporteResultadosNo10-JUL2010PAMAFRO_1.pdf.

Parham, P.E., Michael, E., 2010. Modeling the effects of weather and climate change on malaria transmission. Environ. Health Perspect. 118 (5), 620–626. https://doi.org/10.1289/ehp.0901256.

Patz, J.A., Campbell-Lendrum, D., Holloway, T., Foley, J.A., 2005. Impact of regional climate change on human health. Nature 438 (7066), 310–317. https://doi.org/10.1038/nature04188.

Patz, J.A., Olson, S.H., 2006. Malaria risk and temperature: influences from global climate change and local land use practices. Proceedings of the National Academy of Sciences 103 (15), 5635–5636. https://doi.org/10.1073/pnas.0601493103.

Patz, J.A., Strzepek, K., Lele, S., Hedden, M., Greene, S., Noden, B., Beier, J.C., 1998. Predicting key malaria transmission factors, biting and entomological inoculation rates, using modelled soil moisture in Kenya. Trop. Med. Int. Health: TM & IH 3 (10), 818–827.

Reinbold-Wasson, D.D., Sardelis, M.R., Jones, J.W., Watts, D.M., Fernandez, R., Carbajal, F., Pecor, J.E., Calampa, C., Klein, T.A., Turell, M.J., 2012. Determinants of Anopheles seasonal distribution patterns across a forest to periurban

gradient near Iquitos, Peru. Am. J. Trop. Med. Hyg. 86 (3), 459–463. http://doi:10.4269/ajtmh.2012.11-0547.

Ren, Z., Wang, D., Hwang, J., Bennett, A., Sturrock, H.J.W., Ma, A., Wang, J., 2015. Spatial-temporal variation and primary ecological drivers of Anopheles sinensis human biting rates in malaria epidemic-prone regions of China. PLoS ONE 10 (1). https://doi.org/10.1371/journal.pone.0116932.

Reichle, R.H., Koster, R.D., De Lannoy, G.J.M., Forman, B.A., Liu, Q., Mahanama, S.P.P., Touré, A., 2011. Assessment and enhancement of MERRA land surface hydrology estimates. J. Clim. 24 (24), 6322–6338. https://doi.org/10.1175/JCLI-d-10-05033.1.

Roper, M.H., Torres, R.S., Goicochea, C.G., Andersen, E.M., Guarda, J.S., Calampa, C., Hightower, A.W., Magill, A.J., 2000. The epidemiology of malaria in an epidemic area of the Peruvian Amazon. Am. J. Trop. Med. Hyg. 62 (2), 247–256. Retrieved from http://www.ajtmh.org/content/62/2/247.full.pdf.

Rienecker, M.M., Suarez, M.J., Gelaro, R., Todling, R., Bacmeister, J., Liu, E., Bosilovich, M.G., Schubert, S.D., Lawrence, T., Kim, G., Bloom, S., Chen, J., Collins, D., Conaty, A., da Silva, A., Gu, Wei., Joiner, J., Koster, R.D., Lucchesi, R., Molod, A., Owens, T., Pawson, S., Pegion, P., Redder, C.R., Reichle, R., Robertson, F.R., Ruddick, A.G., Sienkiewicz, M., Woollen, J., 2011. MERRA: NASA's modern-era retrospective analysis for research and applications. J.Clim. 24 (14), 3624–3648. https://doi.org/10.1175/JCLI-d-11-00015.1.

Sinka, M.E., Bangs, M.J., Manguin, S., Rubio-Palis, Y., Chareonviriyaphap, T., Coetzee, M., Mbogo, C.M., Hemingway, J., Patil, A.P., Temperley, W.H., Gething, P.W., Kabaria, C.W., Burkot, T.R., Harbach, R.E., Hay, S.I., 2012. A global map of dominant malaria vectors. Parasite Vectors 5 (69). https://doi.org/10.1186/1756-3305-5-69.

STATA, 2013. Stata multilevel mixed-effects reference manual release 13 Retrieved from https://www.stata.com/manuals13/me.pdf.

Tuteja, R., 2007. Malaria – an overview. FEBS J. 274 (18), 4670–4679. https://doi.org/10.1111/j.1742-4658.2007.05997.x.

Vittor, A.Y., Gilman, R.H., Tielsch, J., Glass, G., Shields, T., Lozano, W.S., Patz, J.A., 2006. The effect of deforestation on the human-biting rate of Anopheles darlingi, the primary vector of falciparum malaria in the Peruvian Amazon. Am. J.Trop. Med. Hyg. 74 (1), 3–11.

World Health Organization, WHO |world malaria report 2015, 2015, Retrieved March 16, 2016, from http://apps.who.int/iris/bitstream/10665/200018/1/9789241565158_eng.pdf?ua=1.

Zaitchik, B., Feingold, B., Spangler, K., Kosek, M., 2012. Towards spatially explicit malaria risk models for the Peruvian Amazon Retrieved March 16, 2015, from http://www.isprs.org/proceedings/XXXVIII/8-C23/pdf/Zaitchik.pdf.